ELSEVIER

Int. J. Therm. Sci. 41 (2002) 29–40

International Journal of Thermal Sciences

Influence of heat transfer on gas and water transport in fuel cells

Nedjib Djilali *, Dongming Lu

Institute for Integrated Energy Systems, University of Victoria, P.O. Box 3055, Victoria, BC, V8W 3P6 Canada

Received 2 May 2000; accepted 6 February 2001

Abstract

An analysis of transport phenomena in a proton exchange membrane fuel cell (PEMFC) is presented, with a focus on the modelling and assessment of non-isothermal and non-isobaric effects that have been neglected in previous studies. A model is formulated for a complete fuel cell taking into account diffusion through the porous electrodes of the humidified fuel (H_2, CO_2 and $H_2O^{(v)}$) and oxidant gases (O_2, N_2 and $H_2O^{(v)}$); the convective and electro-osmotic transport of liquid water in the electrodes and the membrane; and heat generation and transfer in the fuel cell. The thermodynamic equilibrium potential is calculated using the Nernst equation, and reaction kinetics is determined using the Butler–Volmer equation. Non-uniform distribution of gas pressure in the porous gas-diffusing electrodes and micro-hydrodynamics in very small pores (Knudsen diffusion) are also taken into account.

The model is solved numerically to analyze fuel cell performance and water transport over a range of operating current densities. Non-uniform temperature and pressure distributions are found to have a large impact on the predicted liquid water and vapour fluxes in the anode and cathode diffusion layers. In particular, the results indicate that water management requirements (i.e., humidification or water removal) to prevent potential membrane dehydration or electrode flooding are much more conservative than predicted assuming isothermal conditions. Finally, it is found that, in the range of permeabilities of the porous electrodes used in PEMFCs (10^{-16}–10^{-17} m^2), Knudsen diffusion has to be taken into account in modelling gas transport.

Keywords: Fuel cells; Energy conversion; Heat transfer; Mass transfer; Electrochemistry; Porous media; Simulation

1. Introduction

Fuel cells (FCs) are electrochemical devices that convert directly into electricity the chemical energy of reaction of a fuel and an oxidant (usually hydrogen and oxygen). In contrast with batteries, which are energy storage device, fuel cells provide power *continuously*, as long as supplied with fuel. Since the only by-products of the electrochemical reaction in a fuel cell are heat and water, FC technology offers the prospect of zero-emission energy production for applications ranging from stationary power generation for electric utilities, to urban transportation. In this paper, we consider Proton-Exchange Membrane Fuel Cells (PEMFCs). Low operating temperatures ($\approx 80\,^{\circ}C$) and a relatively simple design make PEMFCs strong candidates to provide power for a broad range of systems, including the next generation of non-polluting automobiles, distributed power generation, and portable electronic appliances. The feasibility and potential of PEMFC technology has for instance been demonstrated in the Ballard transit bus [1].

A PEMFC consists of a polymer electrolyte, sandwiched between two electrodes to form a membrane-electrode assembly (MEA). The MEA is placed between two graphite bipolar plates with machined groves that provide flow channels for the distribution of fuel (hydrogen) and oxidant (oxigen from air) as shown schematically in Fig. 1. To produce the desired level of power, single cells are connected in series to form a fuel cell *stack*. The MEA which is at the heart of a single cell consists of a perfluorinated polymer backbone with sulphonic acid side chains. Such membranes are highly resistant to chemical attacks, have good mechanical properties, are electronically insulating, and, when well hydrated, are good conductors of H^+ ions. The typical polymer electrolyte thickness is of the order of 200 microns, with a recent trend towards thinner membranes. The electrodes are made of PTFE (Teflon) coated carbon cloth or paper of about 200–300 microns

* Correspondence and reprints.
E-mail address: ndjilali@uvic.ca (N. Djilali).

1290-0729/02/$ – see front matter
PII: S1290-0729(01)01301-1

Nomenclature

C	specific heat	$J\cdot kg^{-1}\cdot K^{-1}$
c	concentration of a species	
D	diffusivity of a component or a gas pair in a mixture	$m^2\cdot s^{-1}$
d	diameter or size	m
E	cell equilibrium potential	V
F	faraday's constant = 96487	$C\cdot mol^{-1}$
h	enthalpy	$J\cdot kg^{-1}$
i	current density	$A\cdot cm^{-2}$
K	thermal conductivity	$W\cdot m^{-1}\cdot K^{-1}$
Kn	Knudsen number	
k	permeability	m^2
M	molecular weight	$kg\cdot kmol^{-1}$
N	molar flux of a species	$kmol\cdot m^{-2}\cdot s^{-1}$
n	stoichiometric coefficient	
p	pressure	Pa
Q	heat transfer rate	$J\cdot s^{-1}$
R	gas constant	$J\cdot kmol^{-1}\cdot K^{-1}$
T	temperature	K
u	velocity	$m\cdot s^{-1}$
x	mole fraction of a species	
y	mass fraction of a species	
Z	charge number of a species	
z	co-ordinate in cell sandwich direction	m

Greek letters

α	voidage	
η	electrode surface potential	V
κ	protonic conductivity	$\Omega^{-1}\cdot m^{-1}$
λ	mean free path of molecules	m
μ	viscosity	$N\cdot s\cdot m^{-2}$
Ψ	volumetric ratio of pores in a membrane or electrode	
ϕ	electric potential	V
ρ	density	$kg\cdot m^{-3}$
σ	electric conductivity	$\Omega^{-1}\cdot m^{-1}$
τ	tortuosity	

Superscripts

d	values in electrode diffusers
eff	effective value
m	values in the membrane
sat	saturation
$*$	dissolved gases
0	reference

Subscripts

a	anode
act	activation
c	cathode
f	ions bonded to the membrane matrix
g	gas phase
gg	Knudsen diffusion
i	species i
ij	gas pair i, j in a mixture
l	liquid water
lg	phase change between liquid and vapor water
ohm	ohmic resistance
p	(i) constant pressure for specific heat, (ii) hydraulic quantity
po	pores
r	reaction
s	superficial values
sol	solid phase
T	thermal diffusion
w	water
ϕ	electronic parameter
0	inlet values

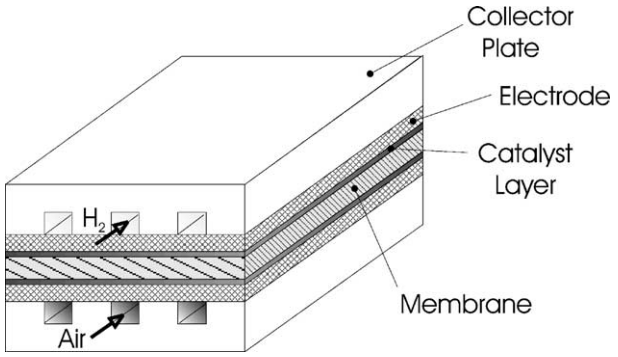

Fig. 1. Schematic of a PEM Fuel Cell.

thickness. The porous structure allows diffusion of the fuel and oxidant gases, evacuation of the product water thanks to the hydrophobic properties of the PTFE. The solid carbon matrix allows collection and flow of the electrons. Another key element in the structure of the MEA is the interface between the membrane and the electrodes, consisting of a platinum catalysts, in the form of very fine particles supported on larger carbon black particles. This structure maximizes the contact area between the catalyst and the reactants. This catalyst is applied directly to the carbon paper or cloth electrode, and PTFE is often added to ensure that product water is expelled to the electrode-gas channel interface where it can evaporate. Many variants exist for the structure of the materials, and the construction of the MEA and bipolar plates; interested readers are referred to, e.g., Larminie and Dicks [2].

The operating principle of a PEMFC is illustrated in Fig. 2. At the anode, fuel (H_2) is oxidized liberating electrons and producing protons. The free electrons flow to the cathode, via an external circuit, where they combine

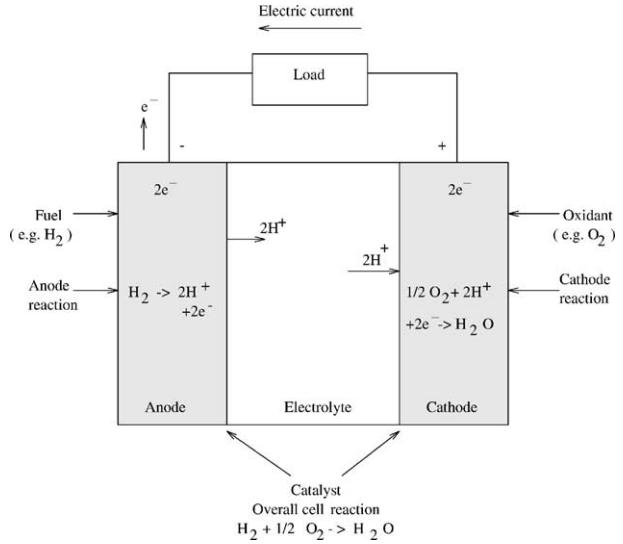

Fig. 2. Operating principle of a proton exchange membrane fuel cell.

with the protons and the dissolved oxidant O_2 to produce water and heat. The electric circuit is completed by the transfer of protons from the anode to the cathode via the solid electrolyte (membrane). The overall reaction at the anode and cathode is given by

$$2H_2 \rightarrow 4H^+ + 4e^- \quad \text{(I)}$$

$$O_2 + 4H^+ + 4e^- \rightarrow 2H_2O(+\text{Heat}) \quad \text{(II)}$$

Several coupled fluid flow, heat and mass transport processes occur in a fuel cell. Two particularly important issues are

(i) thermal and water management, and
(ii) mass transport limitations.

Water management ensures that the polymer electrolyte membrane remains fully hydrated to ensure good ionic conductivity and performance. Water content is determined by the balance between water production with three water transport processes: electro-osmotic drag of water, associated with proton migration from anode to cathode; back diffusion from the cathode; and diffusion of water to/from the oxidant/fuel gas streams. Without control, an imbalance between production and removal rates of water can occur. This results in either dehydration of the membrane, or flooding of the electrodes; both phenomena have a very detrimental effect on performance and fuel cells have to be carefully designed to avoid their occurrence. In current PEMFC designs water content is maintained by humidifying the reactant gas. At higher current densities, the excess product water is removed by convection via the air stream, and the rate of removal is controlled by judiciously adjusting moisture content, pressure drop and temperature in the flow channels. Thermal management is also required to remove the heat produced by the electrochemical reaction (up to $\sim 50\%$ of the energy produced during high power density operation [3]) in order to prevent drying out of the membrane and excessive operating temperatures. The small temperature differentials between the fuel cell stack and the operating environment make thermal management a challenging problem in PEMFCs. In practice forced convection cooling is required. This entails pumping of a coolant into separate cooling channels, thus adding to complexity and cost, and reducing system efficiency. Mass transport limitations are associated with the use of air as the cathodic reactant, and are responsible for a drastic deterioration in performance (polarization) above a certain current density. This is attributed to the lack of oxygen reaching the catalyst, creating oxygen under-stoichiometry or "starvation" at the cathode. In practice, this problem is alleviated by pressurizing the air, again at the cost of reduced system efficiency.

Several modelling studies have been undertaken to investigate the water transport mechanisms and/or thermal effects in fuel cells and to provide guidance for design and optimization. The problems are challenging and involve multi-component and multi-phase flow, heat and mass transfer in porous media with electro-chemical reactions. The models of Verbrugge and Hill [4], Springer et. al. [5], Bernardi and Verbrugge [6,7], Fuller and Newman [8], Nguyen and White [9], and West and Fuller [10], and more recently Wohr et al. [11] have provided very useful insight and reasonable predictions of the cell performance under controlled laboratory conditions. These models are, however, limited by the isothermal assumption (in Ref. [8], thermal gradients are only accounted for along the flow channels using a global energy balance) and, except in [11], the neglect of the potentially significant gas pressure drop within the electrodes. Further, with the exception of the model of Bernardi and Verbrugge [7], all the models are formulated for the membrane or membrane-cathode assembly only. Although FC polarization caused by anode overpotential is often negligible, due to the relatively fast transport and reaction rates of H_2, the anode transport processes may have to be accounted for in order to obtain a reliable estimate of water balance in a fuel cell, since transport of water in the anode can be in either vapour or liquid phase due to humidification, evaporation and removal of the product water.

Thermal and water management is a key issue in PEMFC design and the underlying heat and mass transport processes are coupled. The thermal gradients within a fuel cell are sufficiently large to warrant an investigation of the impact of non-isothermal conditions on water flux predictions. The omission of gas pressure gradients in an electrode is based on the argument that the gas viscosity μ_g is usually an order of magnitude less than that of liquid water, and hence the associated pressure drop $\mathrm{d}p_g/\mathrm{d}z = -u_g(\mu_g/k_{gs}^d)$ is negligible. Further examination reveals that the gas velocity in an electrode is often one or two orders of magnitude faster than that associated with liquid water transport, and the differential in gas pressure in fuel cells and/or its effect on transport processes may, therefore, be important.

Based on the above review of transport processes in fuel cells and previous theoretical studies in this area, the objectives of this work are then to assess the significance of non-isothermal and non-isobaric effects on performance and on water management, and to develop a model that can serve as a basis for more comprehensive simulations and design analyses. The model presented consists of a complete PEM fuel cell, including the anode diffusion layer neglected in most previous studies. The model is implemented numerically and one-dimensional simulations are presented over a range of parameters to investigate the effect of temperature and gas pressure gradients on fuel cell performance and water management. This work is the first theoretical investigation on the effect of non-uniform distribution of temperature and gas pressure on mass transport in PEM fuel cells.

2. Mathematical formulation

A single PEM fuel cell, shown in Fig. 3 is considered. The fuel cell is assumed to operate under steady state conditions. The focus of this work is to assess the relative importance of non-isothermal and non-isobaric effects, and following the bulk of the models available in the literature we consider the transport processes to be one-dimensional (z-direction) in the membrane-electrode assembly. Two-dimensional effects are discussed in Ref. [12]. The local heat transfer rates between fluids, and between fluid and solid phases are sufficiently high for the various phases to have a homogeneous local temperature, i.e., $T_g(z) = T_l(z) = T_{sol}(z) = T(z)$. Gases in the electrodes are assumed perfect and saturated with moisture. It is also assumed that the diffusion of dissolved gases in the membrane and the effect of dissolved gases on water balance is negligible. The modelling of both membrane and gas diffusion electrodes follows that of Bernardi and Verbrugge [6,7] with extensions to account for heat transfer and pressure gradients. Water and gas transport are considered to take place in separate pores with no interaction. Finally, the catalyst layers, which are much thinner than either the electrode diffuser or membrane, are treated as interfaces in this study.

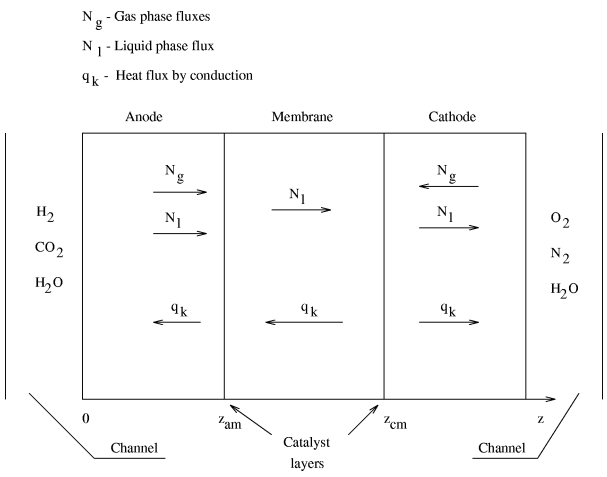

Fig. 3. Co-ordinate system and sign convention for the various fluxes used in the PEMFC model.

The following transport phenomena are taken into account:

- multi-component diffusion of gaseous species through the porous anode and cathode, allowing for the effect of non-uniform gas pressure and cell temperature, and Knudsen diffusion;
- flow of water in both liquid and vapour phases through anode and cathode;
- transport of electrons through the carbon electrodes;
- migration of proton through the membrane;
- transport of water through the membrane via diffusion and electro-osmotic convection;
- electrochemical reaction at the catalyst layer interface;
- heat transfer in all the components of the cell.

The basic equations used in the model are given below and are complemented with a detailed description of the mathematical model in Appendix A. The coordinate system and the sign convention for the various fluxes in the cell are illustrated in Fig. 3, and the symbols are described in the Nomenclature. The species indices $(1, 2, 3)$ correspond respectively to (H_2, CO_2, H_2O^v) in the anode and (O_2, N_2, H_2O^v) in the cathode.

The diffusion of the multi-component gases through the electrodes is represented using the following mass balance equation (see Ref. [13])

$$\frac{\mathrm{d}x_{ig}}{\mathrm{d}z} = \sum_{j=1}^{3} \frac{RT}{p_g D_{ij}^{\mathrm{eff}}} (x_{ig} N_{jg} - x_{jg} N_{ig}) + A_i \qquad i = 2, 3 \tag{1}$$

with

$$A_i = \frac{(y_{ig} - x_{ig})}{p_g} \frac{\mathrm{d}p_g}{\mathrm{d}z} + \sum_{j=1}^{3} \left[\frac{x_{ig} x_{jg}}{\rho_g D_{ij}^{\mathrm{eff}}} \left(\frac{D_{Tj}}{y_{jg}} - \frac{D_{Ti}}{y_{ig}} \right) \right] \frac{1}{T} \frac{\mathrm{d}T}{\mathrm{d}z} \tag{2}$$

The first and second terms on the right hand side of equation (2) represent the effect of gas pressure gradient and the Soret effect (thermal diffusion due to temperature gradients), respectively. Under isothermal and isobaric conditions $A_i = 0$, and equation (1) reduces to the well-known Stefan–Maxwell equation, used in many of the previous modeling studies discussed in the Introduction.

The gas mixture flow in the porous electrodes is governed by

$$u_g = -\left(\frac{k_{gs}^{\mathrm{d}}}{\mu_g} + \alpha \Psi \tau \frac{D_{gg}}{p_g} \right) \frac{\mathrm{d}p_g}{\mathrm{d}z} \tag{3}$$

where the first term on the right is the Darcy pressure drop, and the second accounts for Knudsen diffusion [13], i.e., the diffusion process associated with the collision of individual gas molecules with the walls of the pores. This effect becomes significant when the Knudsen number (ratio of molecular mean free path to pore diameter) $Kn = \lambda_g/d_{po}$ is of order one or greater. An estimate of Kn under practical cell operating conditions, shows that this usually occurs for the gases in a PEMFC when the permeability $k_{gs}^{d} \lesssim 10^{-16}$–$10^{-17}$ m^2. For $\lambda_g/d_{po} \ll 1$ the Knudsen diffusion effect can be neglected, and equation (3) reduces to Darcy's law.

The liquid water transport in the electrodes is governed by Darcy's law

$$u_{l,s}^{d} = -\frac{k_{ps}^{d}}{\mu_l}\frac{dp_l}{dz} \tag{4}$$

and liquid water flow in the membrane is governed by the Schlögl equation, where, in addition to the Darcy pressure drop, a term that accounts for the electro-osmotic drag of water associated with proton migration is included [14]

$$u_l^{m} = \frac{k_\phi}{\mu_l} Z_f c_f F \frac{d\phi}{dz} - \frac{k_p^{m}}{\mu_l}\frac{dp_l}{dz} \tag{5}$$

The Knudsen diffusion process is negligible for liquid water ($\lambda_l/d_{po} \ll 1$).

The flux of protons migrating through the membrane is given by the Nernst–Planck equation [15]

$$N_i = -Z_i \frac{F}{RT} D_i c_i \frac{d\phi}{dz} - D_i \frac{dc_i}{dz} + c_i u_l^{m}$$
$$i = 1, 2, \ldots, m \tag{6}$$

where the three terms on the right hand side represent, respectively, the fluxes due to the electric field, the concentration gradients, and the convective transport. The flow of charged species is related to electric current by

$$i = F \sum_{i=1}^{m} Z_i N_i \tag{7}$$

The reaction kinetics is taken to be first order and described by the Butler–Volmer equation [16]

$$i = i_0\left[e^{-\alpha n F \eta/RT} - e^{(1-\alpha) n F \eta/RT}\right] \tag{8}$$

where the exchange current density i_0 is a function of temperature and reactant concentration, and is given by:

$$i_0 = i_0^{ref}\left(\frac{C_{O_2}}{C_{O_2}^{ref}}\right)^{\gamma_{O_2}}\left(\frac{C_{H^+}}{C_{H^+}^{ref}}\right)^{\gamma_{H^+}} \tag{9}$$

The concentration of the hydrogen protons can be assumed constant throughout the reaction layer, so that the second term of equation (9) is equal to unity. The reference exchange current density i_0^{ref} and the transfer coefficient α are taken as 0.6 A·cm^{-2} and 0.5 for the anode reaction layer, and 4.4×10^{-7} A·cm^{-2} and 1 for the cathode reaction layer.

The equations governing heat transfer in a fuel cell are obtained from an energy balance in the fuel cell; these equations take the following form for the membrane and electrode respectively,

$$\Psi^{m} \rho_l u_l^{m} C_{p,l} \frac{dT}{dz}$$
$$= \left[\Psi^{m} K_l + \left(1 - \Psi^{m}\right) K_{sol}^{m}\right]\frac{d^2T}{dz^2} + \frac{i^2}{\sigma_{sol}^{m}} \tag{10}$$

$$\left(\sum_{j=1}^{3} \rho_{jg} u_{jg} C_{p,jg} + \rho_l u_{l,s}^{d} C_{p,l}\right)\frac{dT}{dz}$$
$$= \left[\Psi^{d}\left(\alpha K_g + (1-\alpha) K_l\right) + \left(1 - \Psi^{d}\right) K_{sol}^{d}\right]\frac{d^2T}{dz^2}$$
$$- \alpha \Psi^{d} \frac{dT\,D}{dz} + \frac{i^2}{\sigma_{sol}^{d}} + Q_{lg} \tag{11}$$

where the source terms i^2/σ_{sol} are associated with Ohmic heating and phase change, and $T\,D$ represents the Dufour effect (see Appendix A).

The equations expressing mass conservation for species, current continuity, and energy conservation together with auxiliary equations (equation of state for gases, equilibrium potential of a cell) are combined with the above equations to obtain the complete model. The complete set of governing equations and associated boundary conditions are given in Appendix A.

The coupled, non-linear set of governing equations is discretized using a staggered-grid finite volume method. The equations are solved numerically for x_{ig}, N_{ig}, p_g, $u_{l,s}^{d}$, u_l^{m}, p_l, ϕ, and T using a fully implicit iterative solution algorithm with under-relaxation. At each iteration level, the system of algebraic equations is solved using the standard Thomas algorithm for tri-diagonal matrix inversion. The iterations are stopped and the solution considered converged based on a check of the overall mass and energy balances. The influence of grid resolution on the accuracy of the numerical solution was investigated over a range of cell operating conditions using various mesh spacings. A non-uniform grid with 10-9-10 control volumes (corresponding to anode-membrane-cathode) was found to provide adequate resolution. This grid density was used in all the numerical calculations presented in this paper.

3. Results and discussion

The focus of the numerical simulations presented in this paper is mainly on the effects of temperature and gas pressure gradients on the fuel cell performance and mass transport characteristics, particularly with respect to product water. The physical properties of the membrane and electrodes are the same as those given in Bernardi and Verbrugge [7], subsequently referred to as BV, and the values of the base case operating parameters are given in Table 1; in the discussion "base case" will be used to refer to isothermal and isobaric conditions.

Table 1
Base case conditions and parameters

Parameter	Value
wet membrane thickness	0.023 cm
gas diffusion electrode thickness	0.026 cm
relative humidity of fuel	100%
relative humidity of Air	100%
cell temperature	80 °C
anode stoichiometric flow ratio ψ_a	1.3
cathode stoichiometric flow ratio ψ_c	3.0
$\frac{x_{N_2}}{x_{O_2}}$, channel inlet	$\frac{0.79}{0.21}$
x_{CO_2}, channel inlet	5 ppm
anode chamber pressure p_{a0}	3.0 atm
cathode chamber Pressure p_{c0}	5.0 atm

3.1. Model validation: Isothermal and isobaric conditions

In the limit of uniform temperature ($K \to \infty$) and constant pressure ($\frac{dp_g}{dz} = 0$), the present numerical model is equivalent to the 1-D isothermal model of BV. In order to validate the numerical model, simulations are therefore performed first for constant temperature and gas pressure to allow comparison with the results of BV. Fig. 4 compares the polarization curves (voltage *vs.* current) computed with the two models to the measurements of Ticianelli et. al. [17]. The results of the present model are in good overall agreement with both those of BV and experimental data; the slight difference between the two can be attributed to the different treatments of the catalyst layer and anode: in the present model (i) the catalyst layers are treated as interfaces, and (ii) the anode diffusion layer is included.

The hydraulic pressure profiles obtained with the model at both low and high current densities are almost identical with those of BV as shown in Fig. 5. Examination of the profiles shows reversal of the hydraulic pressure gradients from positive to negative within the anode and cathode as the current density is increased from $i = 0.105$ to 0.6 A·cm^{-2}.

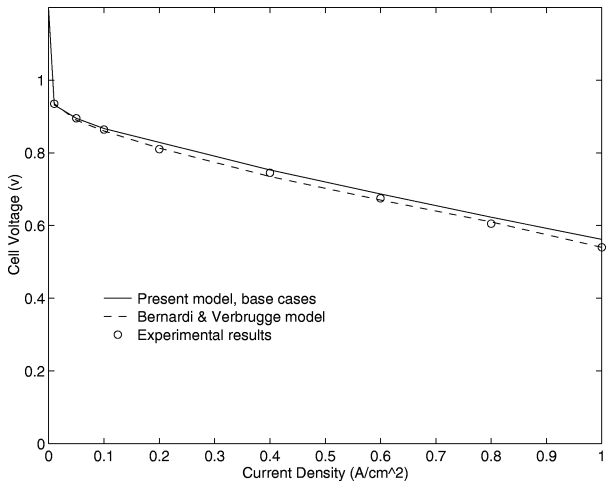

Fig. 4. Comparison of predicted isothermal/isobaric performance curves with the experimental data of Ticianelli et al. [15] and the model of Bernardi and Verbrugge [6].

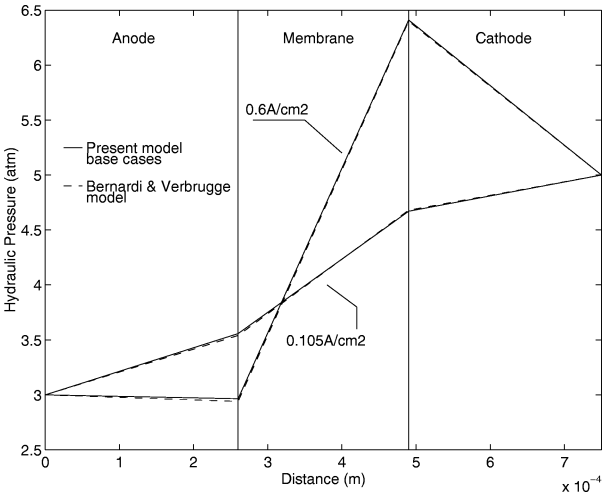

Fig. 5. Comparison of the hydraulic pressure profiles computed under isobaric/isothermal conditions with the results of Bernardi and Verbrugge [6].

The directions of the water fluxes changes accordingly, giving rise to two of the distinct water management regimes documented by BV and by Singh et al. [12].

3.2. Effect of non-uniform temperature and gas pressure

Temperature distribution. Electrodes typically consist of porous carbon paper which has been impregnated with platinum and made hydrophobic by coating with an appropriate compound (usually Teflon^R). The thermal conductivity of the solid portion of an electrode can vary significantly from sample to sample due to the variability in manufacturing techniques, carbon paper grades and amounts of particular compounds. Based on the material composition of the electrodes, the thermal conductivity was estimated to be in the range 0.1 to 1.6 W·m^{-1}·K^{-1}. The numerical simulations are performed for several values in this range.

In order to calculate the temperature field in the fuel cell, a constant temperature boundary condition is imposed at both anode-channel and cathode-channel interfaces. These temperatures are taken here as 80 °C which corresponds to about the middle of the range of usual operating temperatures. Within the iterative procedure, the numerical tolerance to meet the cathode-channel thermal boundary condition is set to ±0.06 °C.

The computed distribution of temperature shown in Fig. 6 clearly illustrate the non-uniform nature of the thermal field, with the higher temperatures achieved inside the cell, particularly at the cathode/membrane interface where the exothermic electrochemical reaction takes place. These results indicate that a typical temperature difference of the order of 1–5 °C may be expected, depending on current density and the thermal conductivity of the electrodes. The higher the current density, the greater the temperature gradient. As the thermal conductivity decreases, temperature distribution becomes more and more non-uniform. We note the slight departure from linearity of the profile (convexity),

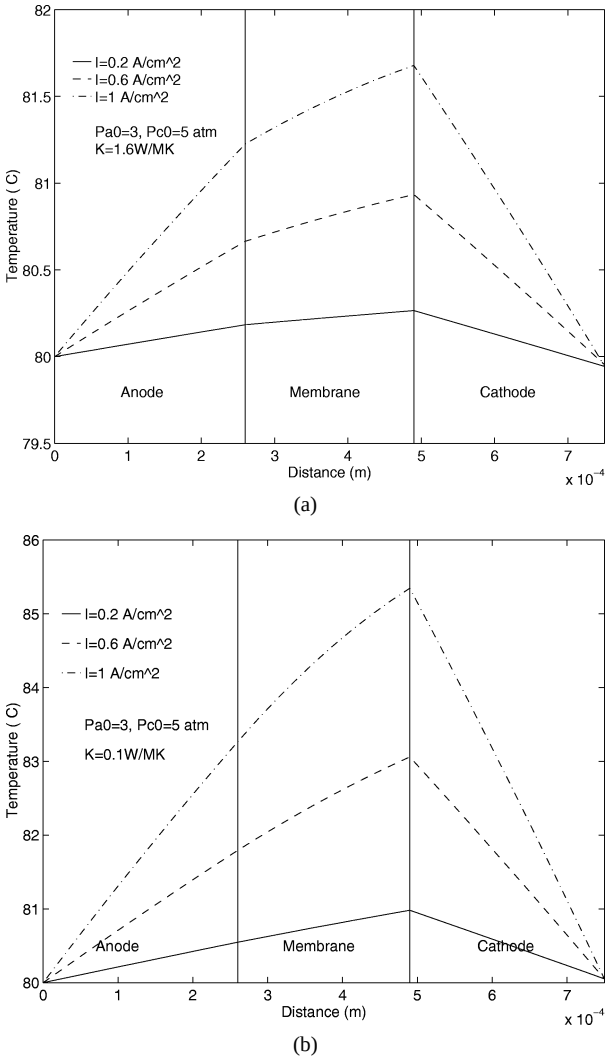

Fig. 6. Computed temperature profiles for different electrode thermal conductivities: (a) $K^{\mathrm{d}}_{\mathrm{sol}} = 1.6\ \mathrm{W{\cdot}m^{-1}{\cdot}K^{-1}}$; (b) $K^{\mathrm{d}}_{\mathrm{sol}} = 0.1\ \mathrm{W{\cdot}m^{-1}{\cdot}K^{-1}}$.

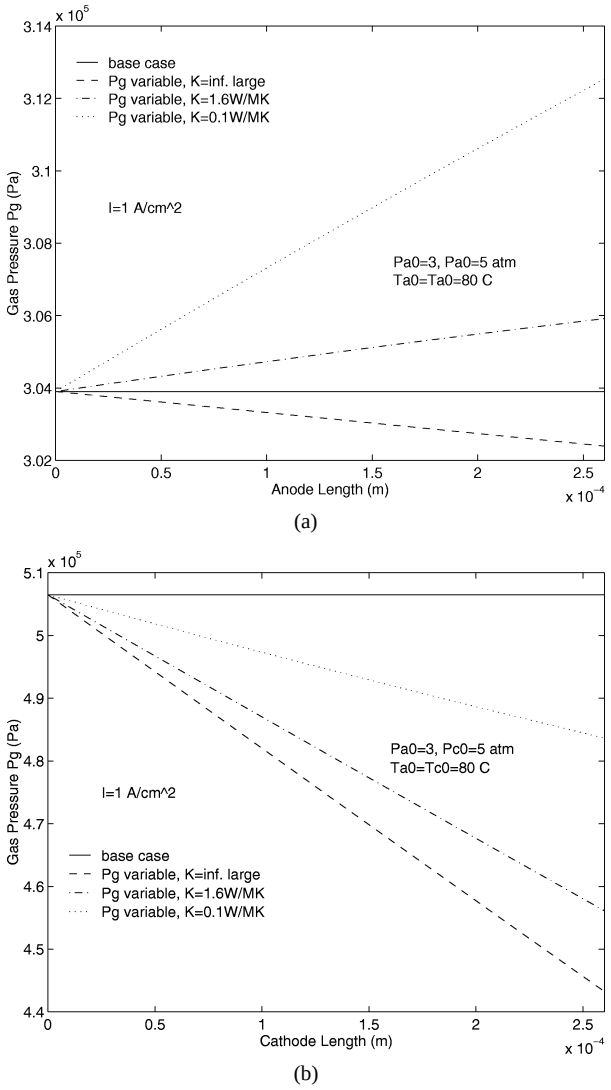

Fig. 7. Gas pressure distribution in the electrodes computed for various thermal conductivities at $i = 1\ \mathrm{A{\cdot}cm^{-2}}$. (a) anode; (b) cathode.

particularly inside the membrane, due to a combination of Joule heating and convective heat transfer associated with the liquid water transport. Overall, the effect of the heat source terms in the energy equation appears minimal.

Gas pressure distribution. Fig. 7 present the computed pressure distribution of the gas mixture in the anode and cathode for a current density of $1\ \mathrm{A{\cdot}cm^{-2}}$. The solid lines correspond to the base case (isothermal and isobaric). Simulations were first performed for isothermal conditions ($K = \infty$) and then for two non-isothermal cases to investigate the effect of heat transfer. As a result of enhanced water evaporation predicted when thermal gradients are taken into account, temperature non-uniformity compensates the Darcy isothermal pressure drop. The resulting pressure gradient is reduced in the cathode, whereas in the anode the negative pressure gradient obtained under isothermal conditions becomes positive when thermal gradients are taken into account. Nonlinear effects become noticeable at the highest conductivity ($K = 1.6\ \mathrm{W{\cdot}m^{-1}{\cdot}K^{-1}}$). The difference between the liquid and gas phases pressures sustained in the porous electrodes is illustrated in Fig. 8.

The effects of T and p_{g} gradients on performance. Fig. 9 shows the polarization curves obtained under various assumptions. It appears that the effect of temperature and gas pressure gradients on the cell output is insignificant at low current densities and minimal at higher ones. This is reasonable in view of the relatively small temperature and gas pressure differentials shown in the previous section, but it should be stressed that the current model does not account for potential dehydration of the membrane, and thus the predicted performance curve assume adequate water management. In the next subsection, it will be shown that the predicted humidification requirements to achieve this are quite different depending whether thermal and pressure gradients are taken into account or not.

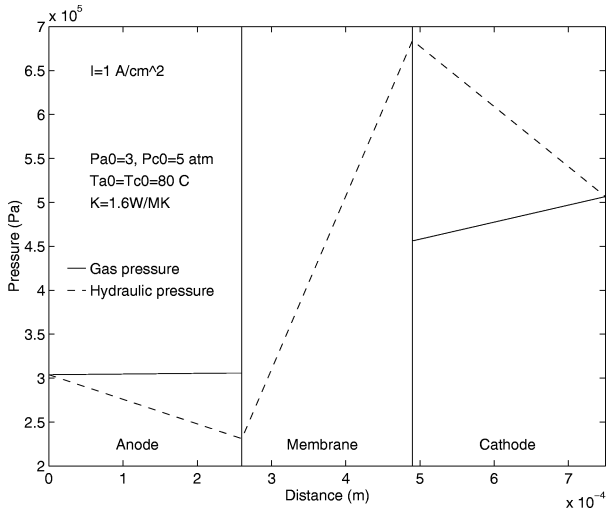

Fig. 8. Comparison of gas and liquid water pressure profiles in the membrane-electrode assembly.

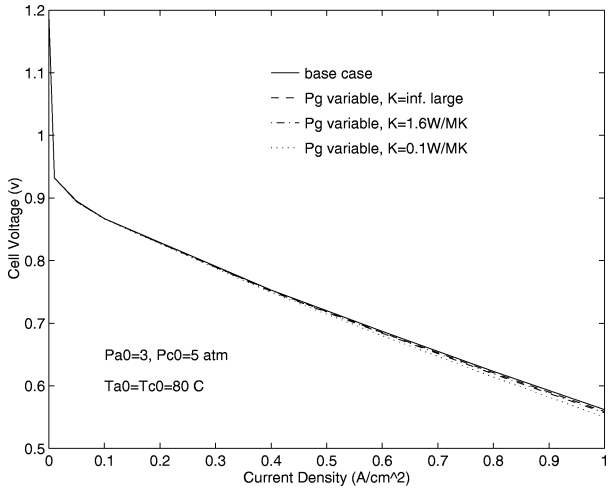

Fig. 9. Direct effect of non-uniform temperature and pressure on predicted fuel cell performance.

The various contributions to cell potential loss are plotted in Fig. 10 over a range of current densities. The cathode overpotential appears to be the dominant factor in cell performance, followed by membrane resistance and then by ohmic losses. The electrodes concentration potentials are negligible at most practical current densities, especially for the anode. Dehydration of the membrane would impact severely on membrane resistance, which is already the second most significant loss contributor.

Effects of T and p_g gradients on water transport. Fig. 11 shows the computed vapour and liquid water fluxes at the anode-channel boundary. We note that the negative liquid water flux (flow from cathode to anode) under open circuit conditions (zero current) is due to the differential pressure between anode and cathode gas streams. In contrast with the polarization results, T and p_g gradients have both a significant influence on water transport in the cell, due to the

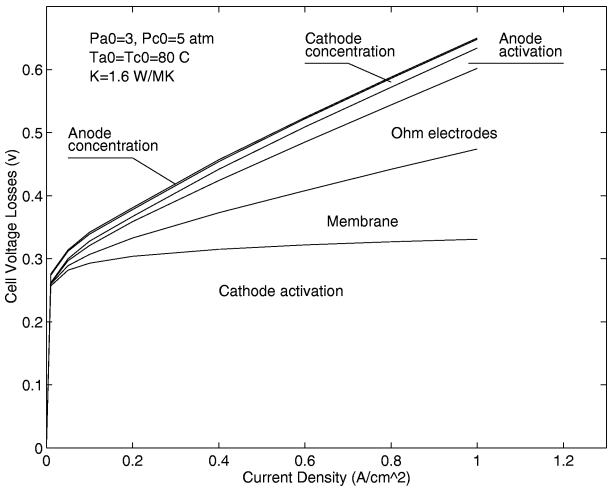

Fig. 10. Computed contributions to overall cell voltage loss.

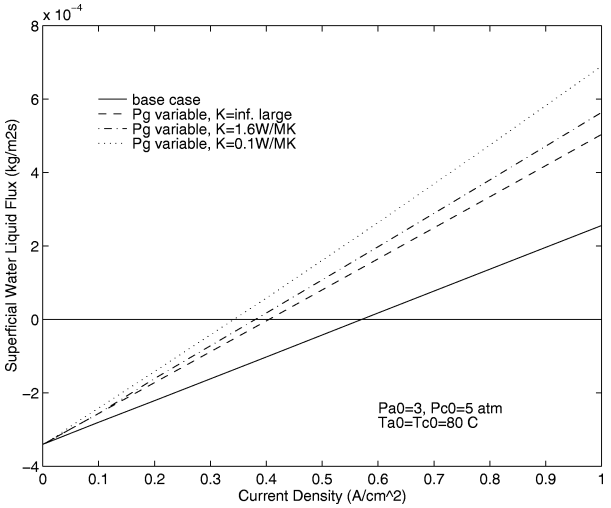

(a)

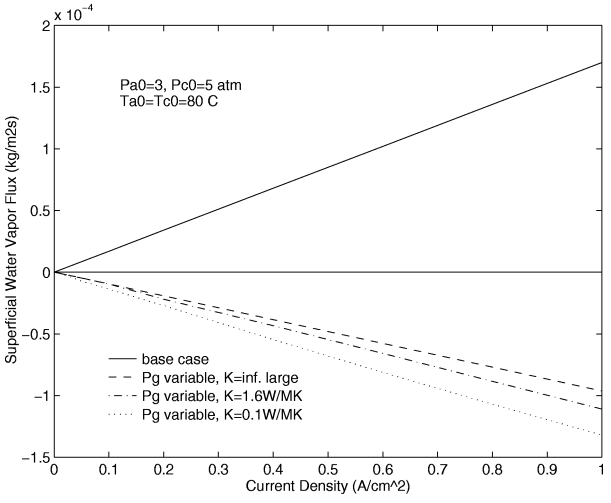

(b)

Fig. 11. Effects of non-uniform temperature and gas pressure on water flux at the anode-channel boundary: (a) liquid water flux; (b) vapour flux.

high sensitivity of water content in a gas carrier to variations of temperature and gas pressure. Compared to the base case, thermal and gas pressure gradients both result in reduced liquid water fluxes out of the anode at low current densities and displace the boundary at which water starts diffusing from anode to cathode to lower current densities. At the higher current densities, the water fluxes obtained under non-isothermal and non-isobaric conditions are 100–200% higher than those obtained under base conditions. Humidification requirements to prevent membrane dehydration are therefore significantly augmented, and are in fact exacerbated by the higher evaporation into the gas mixture favoured by the variation of temperature and gas pressure illustrated in Fig. 11(b).

The liquid water and vapour fluxes on the cathode side are shown in Fig. 12 together with the anode fluxes for one of the non-isothermal/non-isobaric cases ($K = 1.6$ W·m^{-1}·K^{-1}). Examining the liquid water fluxes at the two boundaries, three regimes can be identified:

- Liquid water when $i \leqslant 0.23$ A·cm^{-2}, liquid water flows from cathode to anode. This indicates that additional liquid water is required at the cathode-channel interface while there are no humidification requirements at the anode side since water is removed through the anode.
- when 0.23 A·cm^{-2} $\leqslant i \leqslant$ 0.38 A·cm^{-2}, liquid water flows out of both anode and cathode. The water produced by the O_2 reduction reaction is partitioned. Hence there is no need for humidification at either side of the fuel cell sandwich.
- when $i \geqslant 0.38$ A·cm^{-2}, liquid water flows from the anode to the cathode. Hence humidification is required at the anode side to prevent the membrane from dehydration.

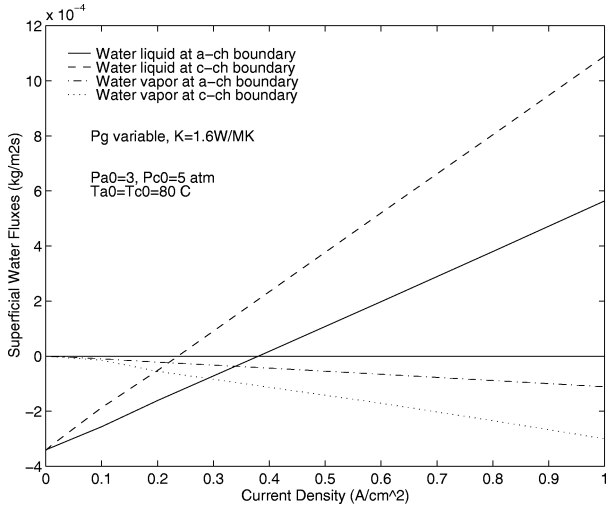

Fig. 12. Variation with current density of water fluxes at anode-channel and cathode-channel boundaries. Non-isothermal ($K^{\mathrm{d}}_{\mathrm{sol}} = 1.6$ W·m^{-1}·K^{-1}) and non-isobaric computations.

These regimes have been observed by BV but with significantly different boundaries. The current density separating regimes 1 and 2 obtained by BV is approximately 0.15 A·cm^{-2}, while that demarcating regimes 2 and 3 is approximately 0.55 A·cm^{-2}. The present model in the isothermal/isobaric limits also obtains similar results. The effect of temperature and gas pressure gradients is to shift the boundaries of regimes 1-2 and 2-3 to higher and lower current densities respectively, thus narrowing the range of regime 2. The overall predicted water management requirements are more conservative, with humidification beginning to be required at a lower current density, and significantly increased amounts of hydration required at higher current densities.

An interesting observation is that water vapour flows out of both anode and cathode at all current densities as shown in Fig. 12. This implies that liquid water may be the most effective phase for humidification. We also note that it is common practice to use a water-saturated reactant stream at a temperature a few or even up to tens of degrees above the cell operating temperature (see, e.g., Bernardi and Verbrugge [7] and Ticianelli et al. [17]). Models using isothermal and isobaric assumptions, which yield vapour fluxes into both sides of the cell, cannot be used to simulate this operating procedure.

The earlier discussion on the relative insensitivity of the fuel cell performance to temperature and pressure gradients has to be considered in the light of the water management requirements. Inadequate humidification, based on isothermal/isobaric assumptions, can cause premature dehydration or flooding and result in severe polarization. We also note that while the very minor contribution of anode concentration overpotential to losses (Fig. 10) justifies performance models which neglect the anode diffusion layer, it is necessary to account for the transport processes in the anode for water transport predictions.

3.3. Knudsen diffusion effect

In porous media, when the permeability becomes sufficiently small the mean free path of the molecules becomes comparable to the pore size ($Kn = \lambda/d_{\mathrm{po}} \gtrsim 1$), and collisions of molecules with the walls start to significantly affect the transport process via Knudsen diffusion. To assess the potential importance of this effect in modelling gas transport processes in the porous electrodes, an order of magnitude estimate of Kn was performed and is presented in Table 2 for a range of electrode permeabilities. The estimate is performed for a nominal pressure of 5 atmosphere (operating pressure of oxidant stream) hold approximately for either oxidant or fuel streams. Kn becomes of order (1) for $k^{\mathrm{d}}_{\mathrm{gs}} < 10^{-16}$–$10^{-17}$ m^2. For a system at lower pressure, the effect is expected to be more important since λ_{g} increases as pressure falls.

Fig. 13 compares the distribution of air pressure in the cathode of a PEMFC calculated considering Knudsen diffusion with that obtained without accounting for the

Table 2
Estimate of Knudesn number, $Kn = \lambda_g/d_{po}$, at 80 °C and 5 atm

k_{gs}^d (m^2)	10^{-13}	10^{-15}	10^{-16}	10^{-17}	10^{-19}
Kn	0.0062	0.062	0.2	0.62	6.2

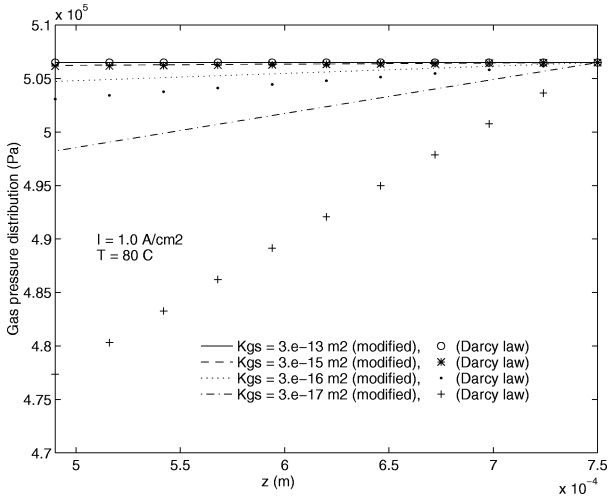

Fig. 13. Effect of Knudsen diffusion on the computed gas pressure distribution in the cathode.

phenomenon. The effect becomes noticeable for $k_{gs}^d = 3 \times 10^{-16}$ m^2 and is very significant for $k_{gs}^d = 3 \times 10^{-17}$ m^2. This is consistent with the estimate presented in Table 2. The permeability values of an electrode reported in the literature are in the range 10^{-16}–10^{-19} m^2, and correspond to values where Knudsen diffusion becomes important. In fact non-physical solutions were obtained with the present model for which the Knudsen term was neglected, and it was found that unrealistic solution were obtained for $k_{gs}^d \leqslant 10^{-18}$ m^2 when the Knudsen term is neglected. The importance of Knudsen diffusion has not been noted or accounted for in previous PEMFC modelling studies.

4. Concluding remarks

A theoretical model of transport phenomena in a PEM fuel cell was formulated. The model takes into account diffusion of humidified fuel and oxidant gases through the porous electrodes, water transport through the electrodes and membrane, as well as heat transfer and gas pressure gradients in the fuel cell. The micro-hydrodynamic phenomena associated with small electrode permeability are also taken into account. The model was implemented in a 1-D code, and a parametric study was performed and results compared and validated against available data. It is found that:

- temperature and gas pressure variations in a fuel cell are important;
- assuming fully hydrated conditions are maintained, polarization is not affected significantly by temperature and pressure non-uniformity;
- water transport is strongly affected by non-uniform temperature and gas pressure distributions, and consequently these have to be taken into account to devise effective water management schemes;
- the model yields more conservative humidification requirements than indicated by isothermal/isobaric models;
- although anode concentration overpotential is negligible, the anode diffusion layer needs to be included in the cell model to properly account for water transport;
- for electrodes with low permeability ($k_{gs}^d \lesssim 10^{-16}$ m^2), Knudsen diffusion becomes significant and has to be taken into account to properly model gas transport.

The focus of this study was to assess the effect of temperature and pressure gradients in fuel cells, an issue that had not been addressed previously. The need to account for these effects has been established in the context of a relatively simplified numerical model. The model does not account for multi-dimensional effects, for convective transport within the flow channels or for variable water content in the membrane (dehydration). Work is under way to incorporate membrane dehydration into the model, to implement the model presented into a multi-dimensional code [12] and to couple it with a CFD model of convective transport in the flow channels.

Acknowledgements

This research was performed under a Collaborative Research and Development (CRD) Grant funded by British Gas Investments (Canada), Ballard Power Systems Inc. and the Natural Sciences and Engineering Research Council of Canada (NSERC).

Appendix A. Complete mathematical model and boundary conditions

Transports in electrodes (anode and cathode)

Gas transport

The gas phase transport in the electrodes is represented by equation (1), presented in the main body of the paper, i.e.,

$$\frac{dx_{ig}}{dz} = \sum_{j=1}^{3} \frac{RT}{p_g D_{ij}^{eff}} (x_{ig} N_{jg} - x_{jg} N_{ig}) + A_i, \; i = 2, 3 \quad \text{(A.1)}$$

where A_i is given by

$$A_i = \frac{(y_{ig} - x_{ig})}{p_g} \frac{dp_g}{dz}$$

$$+\sum_{j=1}^{3}\left[\frac{x_{ig}x_{jg}}{\rho D_{ij}^{\text{eff}}}\left(\frac{D_{\text{T}j}}{y_{jg}}-\frac{D_{\text{T}i}}{y_{ig}}\right)\right]\frac{1}{T}\frac{\mathrm{d}T}{\mathrm{d}z} \tag{A.2}$$

Species $(1, 2, 3)$ represent (H_2, CO_2, H_2O^v) in the case of the anode and (O_2, N_2, H_2O^v) in the case of the cathode.

Applying the principle of mass conservation, we obtain

$$N_{1\text{g}} = \frac{i}{nF} \tag{A.3}$$

$$N_{2\text{g}} = 0 \tag{A.4}$$

where the stoichiometric coefficient is set to $n = 2$ for the anode and $n = 4$ for the cathode.

The reactant gases are assumed to be saturated with water, hence

$$x_{3\text{g}} = x_{\text{wg}}^{\text{sat}} = \frac{p_{\text{w}}^{\text{sat}}}{p_{\text{g}}} \tag{A.5}$$

from which follows

$$\frac{\mathrm{d}x_{3g}}{\mathrm{d}z} = \left(p_{\text{g}}\frac{\mathrm{d}p_{\text{w}}^{\text{sat}}}{\mathrm{d}z} - p_{\text{w}}^{\text{sat}}\frac{\mathrm{d}p_{\text{g}}}{\mathrm{d}z}\right)\Big/ p_{\text{g}}^2 \tag{A.6}$$

The gas mixture also satisfies the condition

$$\sum_{j=1}^{3} x_{j\text{g}} = 1 \tag{A.7}$$

and the flow of a gas mixture in an electrode is governed by Darcy and Knudsen diffusion (see equation (3))

$$u_{\text{g}} = -\left(\frac{k_{\text{gs}}^{\text{d}}}{\mu_{\text{g}}} + \alpha\Psi^{\text{d}}\tau\frac{D_{\text{gg}}}{p_{\text{g}}}\right)\frac{\mathrm{d}p_{\text{g}}}{\mathrm{d}z} \tag{A.8}$$

with

$$u_{\text{g}} = \sum_{j=1}^{3} y_{j\text{g}}u_{j\text{g}} \tag{A.9}$$

Liquid water transport

The transport of liquid water in the porous electrodes is governed by Darcy's law

$$u_{\text{l,s}}^{\text{d}} = -\frac{k_{\text{ps}}^{\text{d}}}{\mu_{\text{l}}}\frac{\mathrm{d}p_{\text{l}}}{\mathrm{d}z} \tag{A.10}$$

and mass conservation of the liquid phase, taking into account phase change,

$$\frac{\mathrm{d}^2p_{\text{l}}}{\mathrm{d}z^2} = \frac{\mu_{\text{l}}}{k_{\text{ps}}^{\text{d}}c_{\text{l}}}\frac{\mathrm{d}N_{3\text{g}}}{\mathrm{d}z} \tag{A.11}$$

Energy conservation

Energy balance in an electrode yields

$$\left(\sum_{j=1}^{3}\rho_{j\text{g}}u_{j\text{g}}C_{\text{p},j\text{g}} + \rho_{\text{l}}u_{\text{l,s}}^{\text{d}}C_{\text{p,l}}\right)\frac{\mathrm{d}T}{\mathrm{d}z}$$

$$= \left[\Psi^{\text{d}}\left(\alpha K_{\text{g}} + (1-\alpha)K_{\text{l}}\right) + \left(1-\Psi^{\text{d}}\right)K_{\text{sol}}^{\text{d}}\right]\frac{\mathrm{d}^2T}{\mathrm{d}z^2}$$

$$-\alpha\Psi^{\text{d}}\frac{\mathrm{d}TD}{\mathrm{d}z} + \frac{i^2}{\sigma_{\text{sol}}^{\text{d}}} + Q_{\text{lg}} \tag{A.12}$$

where the Dufour effect term TD which accounts for heat fluxes associated with concentration gradients and is very small in most cases considered here, is given by

$$TD = RT\sum_{i=1}^{3}\sum_{j=1}^{3}\frac{x_{j\text{g}}D_{\text{T}i}}{M_iD_{ij}^{\text{eff}}}(u_{i\text{g}} - u_{j\text{g}}) \tag{A.13}$$

The last two terms in equation (A.12) correspond to Joule heating an the heat of evaporation, which is obtained from

$$Q_{\text{lg}} = -\frac{\mathrm{d}N_{3\text{g}}}{\mathrm{d}z}\times h_{\text{lg}} \tag{A.14}$$

The thermal conductivity of the gas mixture is calculated using

$$K_{\text{g}} = \sum_{j=1}^{3} x_{j\text{g}}K_{j\text{g}} \tag{A.15}$$

Transports in the membrane

Water and proton transports

Under normal PEMFC operating conditions, water in the membrane is in the liquid phase. Its transport is described by combining the Schlögl and Nernst–Planck equations (5), (6)

$$u_{\text{l}}^{\text{m}} = \frac{-(k_\phi/\mu_{\text{l}}\kappa)Z_{\text{f}}c_{\text{f}}F}{1+(k_\phi/\mu_{\text{l}}\kappa)(Z_{\text{f}}c_{\text{f}}F)^2}i + \frac{-(k_{\text{p}}^{\text{m}}/\mu_{\text{l}})}{1+(k_\phi/\mu_{\text{l}}\kappa)(Z_{\text{f}}c_{\text{f}}F)^2}\frac{\mathrm{d}p_{\text{l}}}{\mathrm{d}z} \tag{A.16}$$

where κ is the proton conductivity and is expressed as

$$\kappa = F^2D_{\text{H}^+}c_{\text{f}}/RT \tag{A.17}$$

The hydraulic pressure may be obtained from the condition of liquid water incompressibility

$$\frac{\mathrm{d}^2p_{\text{l}}}{\mathrm{d}z^2} = 0 \tag{A.18}$$

It can also be shown, from the Nernst–Planck equation (6), electro-neutrality and equation (A.16), that

$$\frac{\mathrm{d}\phi}{\mathrm{d}z} = \frac{-i/\kappa + (Fk_{\text{p}}^{\text{m}}/\mu_{\text{l}}\kappa)Z_{\text{f}}c_{\text{f}}(\mathrm{d}p_{\text{l}}/\mathrm{d}z)}{1+(k_\phi/\mu_{\text{l}}\kappa)(Z_{\text{f}}c_{\text{f}}F)^2} \tag{A.19}$$

Energy conservation

Energy balance in the membrane yields

$$\Psi^{\text{m}}\rho_{\text{l}}u_{\text{l}}^{\text{m}}C_{\text{p,l}}\frac{\mathrm{d}T}{\mathrm{d}z} = \left[\Psi^{\text{m}}K_{\text{l}} + \left(1-\Psi^{\text{m}}\right)K_{\text{sol}}^{\text{m}}\right]\frac{\mathrm{d}^2T}{\mathrm{d}z^2} + \frac{i^2}{\sigma_{\text{sol}}^{\text{m}}} \tag{A.20}$$

where the term $i^2/\sigma_{\text{sol}}^{\text{m}}$ accounts for Joule heating.

Once the operation parameters are specified (p_{a0}, p_{c0}, T_{a0}, T_{c0}, $x_{2\text{a0}}$, $x_{2\text{c0}}$, i), the above equations are solved, subject to the boundary conditions given below, to obtain $x_{i\text{g}}$, $N_{i\text{g}}$, p_{g}, $u_{\text{l,s}}^{\text{d}}$, u_{l}^{m}, p_{l}, p_{l}, ϕ, and T.

Boundary conditions

Refering to Fig. 3, boundary conditions are required at the anode-channel and cathode-channel interfaces (i.e., $z = 0$ and $z = z_c$, respectively), as well as at the anode-membrane interface ($z = z_{am}$) and cathode-membrane interface ($z = z_{cm}$).

At $z = 0$ (Anode–Fuel Channel Interface):

$$x_{ig} = x_{ia0}, \quad i = 2, 3 \tag{A.21}$$

$$p_g = p_l = p_{a0} \tag{A.22}$$

$$T = T_{a0} \tag{A.23}$$

At $z = z_{am}$ (Anode–Membrane Interface):

$$p_l|_{z_{am}^+} = p_l|_{z_{am}^-} \tag{A.24}$$

$$\Psi^m c_l u_l^m|_{z_{am}^+} = \left(N_{3g} + c_l u_{l,s}^d\right)\big|_{z_{am}^-} \tag{A.25}$$

$$T|_{z_{am}^+} = T|_{z_{am}^-} \tag{A.26}$$

$$\left.\frac{dT}{dz}\right|_{z_{am}^+} = \left(\left\{\left[\Psi^d\left(\alpha K_g + (1-\alpha)K_l\right) + \left(1-\Psi^d\right)K_{sol}^d\right]\frac{dT}{dz} + N_{3g}h_{lg}\right\}\Big|_{z_{am}^-} + Q_{ra}\right) \times \left(\Psi^m K_l + \left(1-\Psi^m\right)K_{sol}^m\right)^{-1} \tag{A.27}$$

$$\phi = 0 \tag{A.28}$$

Equation (A.25) is based on mass conservation of water across the anode-membrane interface z_{am}, taking into account phase change; equation (A.27) is obtained from the energy balance across the interface, taking into account phase change and reaction heat.

At $z = z_{cm}$ (Cathode–Membrane Interface):

$$p_l|_{z_{cm}^+} = p_l|_{z_{cm}^-} \tag{A.29}$$

$$\Psi^m c_l u_l^m|_{z_{cm}^-} + \frac{i}{2F} = \left(-N_{3g} + c_l u_{l,s}^d\right)\big|_{z_{cm}^+} \tag{A.30}$$

$$T|_{z_{cm}^+} = T|_{z_{cm}^-} \tag{A.31}$$

$$\left.\frac{dT}{dz}\right|_{z_{cm}^+} = \left(\left[\Psi^m K_l + \left(1-\Psi^m\right)K_{sol}^m\right]\left.\frac{dT}{dz}\right|_{z_{cm}^-} - Q_{rc} - N_{3g}h_{lg}|_{z_{cm}^+}\right) \times \left(\Psi^d\left[\alpha K_g + (1-\alpha)K_l\right] + \left(1-\Psi^d\right)K_{sol}^d\right)^{-1} \tag{A.32}$$

Equations (A.30) and (A.32) are obtained in the same fashion as those at the anode-membrane interface (Equations (A.25), (A.27)), noting that at the cathode-membrane interface, in addition to phase change, water is produced from the electrochemical reaction.

At $z = z_c$ (Cathode–Fuel Channel Interface):

$$x_{ig} = x_{ic0}, \quad i = 2, 3 \tag{A.33}$$

$$p_g = p_l = p_{c0} \tag{A.34}$$

$$T = T_{c0} \tag{A.35}$$

References

[1] K.B. Prater, Solid polymer fuel cell developments at Ballard, J. Power Sources 37 (1992) 181–188.

[2] J. Larminie, A. Dicks, Fuel Cell Systems Explained, Wiley, Chichester, 2000.

[3] R. Mosdale, S. Srinivasan, Analysis of performance and of water management in proton exchange membrane fuel cells, Electrochimica Acta 40 (4) (1995) 413–421.

[4] M.W. Verbrugge, R.F. Hill, Transport phenomena in perfluorosulfonic acid membranes during the passage of current, J. Electrochem. Soc. 137 (4) (1990) 1131–1138.

[5] T.E. Springer, T.A. Zawodzinski, S. Gottesfeld, Polymer electrolyte fuel cell model, J. Electrochem. Soc. 138 (8) (1991) 2334–2342.

[6] D.M. Bernardi, M.W. Verbrugge, Mathematical model of a gas diffusion electrode bonded to a polymer electrolyte, AIChE J. 37 (8) (1991).

[7] D.M. Bernardi, M.W. Verbrugge, A mathematical model of the solid-polymer-electrolyte fuel cell, J. Electrochem. Soc. 139 (9) (1992) 2477–2491.

[8] T.F. Fuller, J. Newman, Water and thermal management in solid-polymer-electrolyte fuel cells, J. Electrochem. Soc. 140 (5) (1993) 1218–1225.

[9] T.V. Nguyen, R.E. White, A water and heat management model for proton-exchange-membrane fuel cells, J. Electrochem. Soc. 140 (8) (1993) 2178–2186.

[10] A.C. West, T.F. Fuller, Influence of rib spacing in proton-exchange membrane electrode assembly, J. Appl. Electrochem. 26 (1996) 557–565.

[11] M. Wohr, K. Bowlin, W. Schnurnberger, M. Fischer, W. Neubrand, G. Eigenberger, Dynamic modelling and simulation of a polymer membrane fuel cell including mass transport limitation, Internat. J. Hydrogen Energy 23 (1998) 213–218.

[12] D. Singh, D.M. Lu, N. Djilali, A two-dimensional analysis of mass transport in proton exchange membrane fuel cells, Internat. J. Engrg. Sci. 37 (1999) 431–452.

[13] R.E. Cunningham, R.J. Williams, Diffusion in Gases and Porous Media, Plenum, New York, 1980.

[14] R. Schlögl, Zur Theorie der Anomalen Osmose, Z. Phys. Chem. 3 (1955) 73–98.

[15] A.J. Appleby, Characteristics of fuel cell systems, in: L. Blomen, M. Mugerwa (Eds.), Fuel Cell Systems, Plenum, New York, 1993, pp. 157–199.

[16] J. Newman, Electrochemical Systems, Prentice-Hall, Englewood Cliffs, NJ, 1973.

[17] E.A. Ticianelli, C.R. Derouin, A. Redondo, S. Srinivasan, Methods to advance technology of proton exchange membrane fuel cells, J. Electrochem. Soc. 135 (9) (1998) 2209–2214.